On the Stochastic Model for InSAR Single Arc Point Scatterer Time Series

Brouwer, Wietske S.; Wang, Yuqing; Van Leijen, Freek J.; Hanssen, Ramon F.

DOI
10.1109/IGARSS52108.2023.10282629

Publication date
2023

Document Version
Final published version

Published in
IGARSS 2023 - 2023 IEEE International Geoscience and Remote Sensing Symposium, Proceedings

IGARSS 2023 - 2023 IEEE International Geoscience and Remote Sensing Symposium | 979-8-3503-2010-7/23/$31.00 ©2023 IEEE | DOI: 10.1109/IGARSS52108.2023.10282629

ON THE STOCHASTIC MODEL FOR INSAR SINGLE ARC POINT SCATTERER TIME SERIES

Wietske S. Brouwer, Yuqing Wang, Freek J. van Leijen, and Ramon F. Hanssen

Delft University of Technology, Department of Geoscience and Remote Sensing
Delft, 2628 CN, The Netherlands

ABSTRACT

InSAR enables the estimation of displacements of (objects on) the earth's surface. To provide reliable estimates, both a stochastic and mathematical model are required. However, the intrinsic problem of InSAR is that both are unknown. Here we derive the Variance-Covariance Matrix (VCM) for double differenced phase observations for an arc, i.e., the phase difference between two points relative to a reference epoch. Using the Normalized Amplitude Dispersion we subdivide the time series in multiple partitions. The method results in a more realistic stochastic model, and consequently more realistic and reliable displacement parameters. The stochastic model also allows to make statements on the precision and reliability of the estimated parameters.

Index Terms— InSAR, Point Scatterers, stochastic model, parameter estimation

1. INTRODUCTION

InSAR (SAR Interferometry) can be used to provide displacement estimates for an arc, formed by two coherent scatterers. Since the original observation is the double-differenced (DD) phase, i.e., the phase difference between the two scatterers, relative to a reference epoch [1], both a proper functional and stochastic model are required to estimate displacement parameters. However, the intrinsic problem of InSAR is that both are unknown.

Using Point Scatterers (PS), it is generally never known exactly from what object the main signal originates, resulting in an unknown kinematic behavior, i.e., functional model. This problem is especially important in the built environment [2]. Regarding the stochastic model, the quality of a phase observation at a single epoch is intrinsically unknown, and each scatterer will have unique scattering properties. In current PSI approaches the quality of the observations is often based on the residuals between the observations and the model evaluated from the estimates [3], [4], which introduces an intricate dependency on the correctness of the functional model. Conceptually, the stochastic model should be known *before* the estimation since it influences the result. Moreover, an independent stochastic model is essential for testing the entire mathematical model [4]. A stochastic model that is chosen too conservatively may lead to sustaining the null hypothesis while it should be rejected. Thus, a proper stochastic model is essential to provide reliable displacement estimates.

2. THE MATHEMATICAL MODEL

The double-differenced phase observation for an arc is the phase difference between two point scatterers i and j, and image d relative to mother image m (where d relates to daughter), and is the sum of different components:

$$\begin{aligned}\underline{\varphi}_{ij}^{md} =& \underline{\varphi}_{j}^{md} - \underline{\varphi}_{i}^{md} \\ =& -2\pi a_{ij}^{md} + \varphi_{ij,D}^{md} + \varphi_{ij,H}^{md} + \varphi_{ij,T}^{md} + \varphi_{ij,S}^{md} + \varphi_{ij,n}^{md},\end{aligned} \tag{1}$$

where $a \in \mathbb{Z}$ is the integer ambiguity, φ_D the displacement phase, and φ_H, φ_T, φ_S, and φ_n the phases due to the (residual) height, temperature, atmospheric delay, and noise, respectively. The signals of interest to be estimated are the (residual) height, displacement and thermal phase. The mathematical model (for the absolute phase) therefore becomes

$$E\{\begin{bmatrix}\underline{\varphi}_{ij}^{m1}\\ \vdots \\ \underline{\varphi}_{ij}^{mD}\end{bmatrix}\} = \underbrace{(D_A|B_T)}_{\varphi_{ij,D}^{md}} + \underbrace{(\alpha_L L|B_{\text{th}})}_{\varphi_{ij,T}^{md}} + \underbrace{(H_{ij}|B_\perp)}_{\varphi_{ij,H}^{md}}; \tag{2}$$

$$\underbrace{D\{\begin{bmatrix}\underline{\varphi}_{ij}^{m1}\\ \vdots \\ \underline{\varphi}_{ij}^{mD}\end{bmatrix}\}}_{\underline{y}} = Q_{\varphi_{ij}} = \underbrace{Q_{\varphi_{ij},\text{atm}}}_{\varphi_{ij,S}^{md}} + \underbrace{Q_{\varphi_{ij},\text{TVC}} + Q_{\varphi_{ij},\text{thn}}}_{\varphi_{ij,n}^{md}}, \tag{3}$$

where $E\{.\}$ is the expectation of the model consisting of three unknown parameters: the relative displacement D_A, relative thermal expansion $\alpha_L L$, and (residual) height H_{ij}. The deformation phase is a function of the temporal baseline B_T. The thermal phase is caused by thermal expansion of the scattering object, as a function of the thermal expansion coefficient α_L and temperature (or thermal baseline B_{th}). The (residual)

height phase, is a function of the perpendicular baseline $B_\perp$. $D\{.\}$ is the dispersion of the model, described by the Variance Covariance Matrix (VCM) $Q_{\varphi_{ij}}$, which is the sum of i) the atmospheric noise $Q_{\varphi_{ij},\text{atm}}$, ii) the thermal noise $Q_{\varphi_{ij},\text{thn}}$, and iii) the Time Variant Clutter (TVC) $Q_{\varphi_{ij},\text{TVC}}$.

2.1. Derivation of the VCM for an arc

With one mother and D daughter acquisitions, the VCM of the SLC phase observations, ψ, for PS i, can be written as

$$Q_{\psi_i} = \begin{bmatrix} \sigma^2_{\psi_i^0} & 0 & \dots & 0 \\ 0 & \sigma^2_{\psi_i^1} & & \vdots \\ \vdots & & \ddots & \\ 0 & \dots & & \sigma^2_{\psi_i^D} \end{bmatrix}, \tag{4}$$

where $\sigma^2_{\psi_i^d}$ is the variance of the SLC phase observation for PS i at epoch d. All three noise components are uncorrelated in time, i.e., the off-diagonal terms are zero. Extending this to an arc, the SLC observations of PS i and j should be combined:

$$D\{\begin{bmatrix} (\underline{\psi}_i^0, \dots, \underline{\psi}_i^D)^T \\ (\underline{\psi}_j^0, \dots, \underline{\psi}_j^D)^T \end{bmatrix}\} = \underbrace{\begin{bmatrix} Q_{\psi_i} & Q_{\psi_i,\psi_j} \\ Q_{\psi_i,\psi_j} & Q_{\psi_j} \end{bmatrix}}_{Q_{\psi_{ij}}}, \tag{5}$$

where Q_{ψ_i,ψ_j} describes the covariance between PS i and j. The VCM for the single difference phase observations in time, i.e., the phases of the interferogram of the daughter acquisition relative to the mother, is then defined as

$$Q_{\text{IFG}_{ij}} = \Lambda\, Q_{\psi_{ij}}\, \Lambda, \text{ with} \tag{6}$$

$$\Lambda = I_2 \otimes \begin{bmatrix} -I_p & e_D & 0 \\ 0 & & -I_q \end{bmatrix}, \tag{7}$$

I the identity matrix, and e_D a vector of ones. p and q depend on the index of the mother image in the stack. With m_i the index of the mother image, $p = m_i - 1$, and $q = D - p$.

The VCM of the DD interferometric phases ϕ is now

$$Q_{\varphi_{ij}} = \Omega\, Q_{\text{IFG}_{ij}}\, \Omega, \text{ with} \tag{8}$$

$$\Omega = \begin{bmatrix} -1 & 1 \end{bmatrix} \otimes I_D. \tag{9}$$

This shows that given the VCMs of the SLC phase observations, and the covariance between the the two PS, the VCM of the DD interferometric phases can easily be derived.

2.2. Atmospheric noise

The atmosphere causes a phase delay on the observed SLC phases mainly depending on turbulent mixing and vertical stratification [1][1]. Since the turbulent atmospheric delay is completely uncorrelated between different acquisitions, all

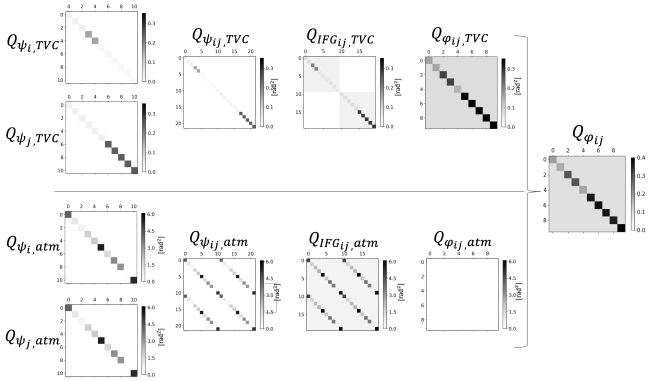

Fig. 1. Approximation of $Q_{\varphi_{ij}}$ as the sum of $Q_{\varphi_{ij},\text{TVC}}$ (above) and $Q_{\varphi_{ij},\text{atm}}$ (below). Column 1: VCM of the SLC phases of point i and j separately, with 11 epochs. For point i the time series was subdivided into three partitions, with one value $\sigma_{\psi,\text{TVC}}$ per partition. $Q_{\psi_{ij}}$ shows the correlation between two points, where we see correlation in the $Q_{\psi_{ij},\text{atm}}$ because of the simulated short arc. $Q_{\text{IFG}_{ij}}$ is the VCM of the single difference (phase difference in time). The difference between the two points result in the Variance-Covariance Matrix (VCM), $Q_{\varphi_{ij}}$, of the double difference phase observations for one arc.

off-diagonal terms in $Q_{\psi_i,\text{atm}}$ are zero [1], see Fig. 1. While the atmosphere is uncorrelated in time, it is correlated in space and therefore $Q_{\psi_i,\psi_j} \neq 0$, and it depends on the distance between the two PS. The covariance values can be approximated with [1]

$$C_{\text{atm}}(l) = \sigma^2_{\text{atm}} \exp(-l^2\omega^2), \tag{10}$$

where l is the arc length (the distance between the two PS) and ω relates to the correlation length of the atmospheric signal l_c, and is defined as $\omega^2 = \ln(2)/l_c^2$. The lower row of Fig.1 shows the theoretical derivation of $Q_{\varphi_{ij},\text{atm}}$ for a short arc. While the atmospheric phase delay for the SLC observations can be quite significant, the variance of the atmospheric phase delay is close to zero for the DD phases since Q_{ψ_i,ψ_j} is almost equal to the variances of the SLC phase delays.

2.3. Thermal noise

The thermal noise is caused by the radar instrument itself and is represented by the Noise Equivalent Sigma Nought (NESN). For Sentinel-1 the NESN has a value around -25 dB [5]. In Fig. 2 the thermal noise is represented by the red arrows.

2.4. Time Variant Clutter

SLC observations of a PS consist of three components i) signal, ii) Time Invariant Clutter (TIC), and iii) Time Variant

[1]For this work, we ignored the influence of the ionosphere.

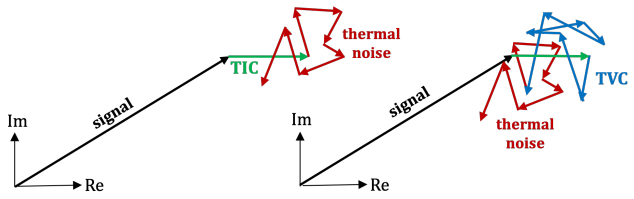

Fig. 2. SLC observation of two PS over time. The black arrow represents the signal of interest, that for this particular case does not change over time. The PS at the left has only Time Invariant Clutter but since the thermal noise differs per acquisition, the observations change over time. The PS at the right has also Time Variant Clutter.

Clutter (TVC). The observed SLC phase for one PS is the sum of all reflective objects within the same resolution cell. For strong PS, there is often one dominant scatterer in the resolution cell with a, *by definition*, coherent signal.[2] Thus, signals from other reflective objects within the same resolution cell can be regarded as noise, or clutter, as they are not necessarily related to the behavior of the main scatterer.

The clutter can be divided in two parts: the Time Invariant Clutter (TIC) and Time Variant Clutter (TVC). The TIC is the clutter that does not change between different acquisitions. An extreme example would be a Corner Reflector (CR) on top of a rough concrete plate. The signal of interest is strong and relates to the CR. However, the concrete plate also causes reflections that do not belong to the signal of interest. When no displacements occur over time, the clutter caused by the concrete plate does not change over time, i.e., it is time *invariant*, see Fig. 2. From the observations it is impossible to distinguish between the *signal* of interest and the TIC, since both are time invariant. Consequently, both terms are attributed to the signal that belongs to the functional model.

The Time Variant Clutter (TVC) does change over time. An example would be a CR in the middle of a meadow. As long as the CR is not moving, the signal does not change over time, whereas the reflections caused by the grass differ per acquisition, see Fig. 2.

2.4.1. VCM for the TVC

As can be seen in Fig. 2, the TVC and thermal noise together contribute to the noise in the SLC phase observations. However, it is not possible to distinguish between the two components from the complex SLC phase observations only. Therefore, from now on the two components will modeled together in $Q_{\varphi_{ij},\text{TVC}}$. Since the TVC and thermal noise vary with time by definition, there is no correlation in time and $Q_{\psi_i,\text{TVC}}$ reduces to a diagonal matrix with variances values for the SLC phases on the diagonal.

[2]A coherent signal is required to estimate the residual height, displacement, and thermal expansion.

To estimate $\sigma_{\psi,\text{TVC}}$, not only the TVC and thermal noise but also the strength of the signal itself is important. The effect of both components will be larger on weak reflections compared to strong reflections. When the contribution of the TVC or thermal noise is significant, this results in a variation in amplitude but the effect on the observed phases depends on the strength of the signal. Therefore the Normalized Amplitude Dispersion (NAD) [6] is a good proxy to estimate $\sigma_{\psi,\text{TVC}}$, with

$$\sigma_{\psi,\text{TVC}} \approx \frac{\sigma_A}{\mu_A} = \text{NAD}, \tag{11}$$

where μ_A is the mean amplitude and σ_A its standard deviation. However, the amplitude of a scatterer may actually vary over time, and consequently so does $\sigma_{\psi,\text{TVC}}$ [7]. Therefore, the time series can be subdivided into multiple partitions, where each partition may have its own behavior, see Fig. 3b. As long as there are enough observations per partition, the NAD and quality of the phase can be estimated for each partition of the time series.

Added to this, the assumption of $\sigma_{\psi,\text{TVC}} \approx \text{NAD}$ only holds when $\text{NAD} < 0.2$ [6], and therefore we derived an empirical relation between the NAD and $\sigma_{\psi,\text{TVC}}$ based on simulations as [3, 6, 8], see Fig. 4. The empirical relation is

$$\sigma_{\psi,\text{TVC}} = a + b\,\text{NAD} + c\,\text{NAD}^2 + d\,\text{NAD}^3, \tag{12}$$

with $a = -7.66 * 10^{-3}$, $b = 1.33$, $c = -3.18$, and $d = 9.35$.

As a result, for each partition of the time series the NAD is calculated with Eq. (11) and accordingly a value for $\sigma_{\psi,\text{TVC}}$ can be approximated with Eq. (12), which can be used to fill the diagonal of $Q_{\psi,\text{TVC}}$. In Fig. 1 we show a theoretical example of the derivation of the VCM containing of the sum of $Q_{\varphi_{ij},\text{TVC}}$ (upper row) and $Q_{\varphi_{ij},\text{atm}}$ (lower row). The first column of Fig. 1 shows this for two points (i and j) defining one arc with different partitions.

3. RESULTS, IMPACT, AND CONCLUSION

Fig. 3 shows an example of the approach applied on real data. The two points of the arc have a distance of 40 meters, and therefore, as is shown in Fig. 1, $Q_{\varphi_{ij},\text{atm}} = 0$, and only $Q_{\varphi_{ij},\text{TVC}}$ is important.

For both points the time series was divided into two partitions (see Fig. 3a and b), with new partitions starting at epoch 235 and 60 for point i and j respectively. Consequently, the NAD and $\sigma_{\psi,\text{TVC}}$ were estimated for each partition, and $Q_{\psi_i,\text{TVC}}$ and $Q_{\psi_j,\text{TVC}}$, and subsequently $Q_{\varphi_{ij},\text{TVC}}$ could be derived, see Fig. 3c. Note the differences in the diagonal terms. The inscribed blue lines represent the values for $\sigma_{\varphi_{ij}}$, using the right axis. It shows that the approximated quality of the DD phase observations for the first 60 epochs ($\sigma_{\varphi_{ij}} = 0.72$ rad) is approximately 1.6 times worse as the phase quality for the other epochs ($\sigma_{\varphi_{ij}} \approx 0.45$ rad).

As a last step, the Line-of-Sight (LoS) velocity of the arc was estimated using $Q^{-1}_{\varphi_{ij}}$ as the weight matrix, and compared

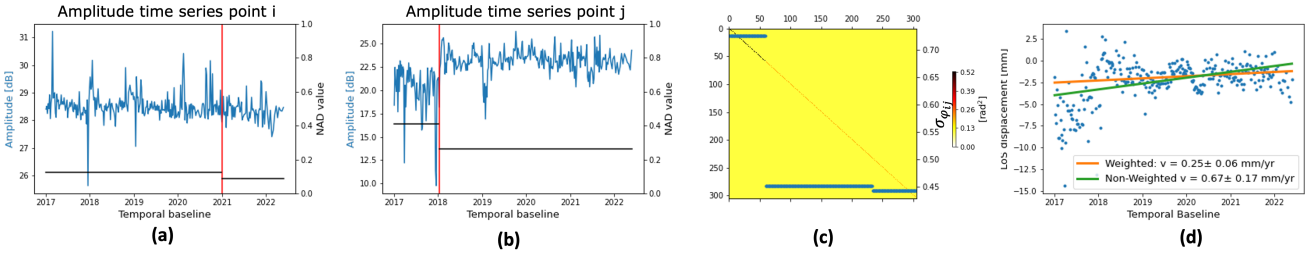

Fig. 3. **(a)** and **(b)**: amplitude time series for points i and j. For both points two partitions are detected. For each partition, the NAD is estimated and visualized by the horizontal black line. From the NAD values, the values for $\sigma_{\psi,\text{TVC}}$ could be calculated with Eq. (12), and consequently the VCM for the arc observations is constructed, **(c)**. We separately visualized the diagonal of $Q_{\varphi_{ij}}$, as values represented by the horizontal blue lines, see the right axis. **(d)** Estimated displacements and estimated velocity using the proper stochastic model (weighted) and conventional model with equal weights for all observations.

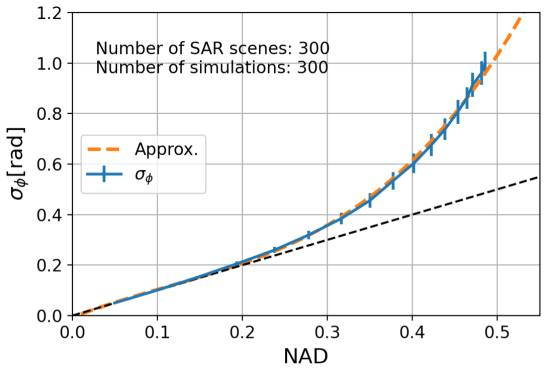

Fig. 4. The relation between the NAD and $\sigma_{\psi,\text{TVC}}$. The blue line shows the values (and error bars) based on simulations of time series with 300 SAR scenes and different noise levels. The striped orange line shows the derived empirical relation between the NAD and $\sigma_{\psi,\text{TVC}}$ from Eq. (12). Figure based on [6].

with the conventional unit weight matrix, see Fig. 3d. We found LoS velocities of 0.25 mm/yr and 0.67 mm/yr for the weighted and non-weighted case respectively.

It can be concluded that using a more realistic stochastic model improves the result. For the first 60 epochs, the spread of the LoS displacements seems to be larger, which is in accordance with the stochastic model. The fitted trend, using weights, is a better representation of the observations. Moreover, using a proper stochastic model allows us to make statements on the precision and reliability of the estimated parameters, which is essential when the results are used for monitoring purposes. Finally, a proper stochastic model is essential for testing purposes.

4. REFERENCES

[1] R. F. Hanssen, *Radar Interferometry: Data Interpretation and Error Analysis*, Kluwer Academic Publishers, Dordrecht, 2001.

[2] B. Van De Kerkhof, V. Pankratius, L. Chang, R. Van Swol, and R.F. Hanssen, "Individual scatterer model learning for satellite interferometry," *IEEE transactions on geoscience and remote sensing*, vol. 58, no. 2, pp. 1273–1280, 2019.

[3] F. J. van Leijen, *Persistent scatterer interferometry based on geodetic estimation theory*, Ph.D. thesis, Delft University of Technology, Delft, the Netherlands, 2014.

[4] L. Chang and R.F. Hanssen, "A probabilistic approach for InSAR time-series postprocessing," *IEEE transactions on geoscience and remote sensing*, vol. 54, no. 1, pp. 421–430, 2015.

[5] R. Torres, I. Navas-Traver, D. Bibby, S. Lokas, P. Snoeij, B. Rommen, S. Osborne, F. Ceba-Vega, P. Potin, and D. Geudtner, "Sentinel-1 SAR system and mission," in *2017 IEEE Radar Conference (RadarConf)*. IEEE, 2017, pp. 1582–1585.

[6] A. Ferretti, C. Prati, and F. Rocca, "Permanent scatterers in SAR interferometry," vol. 39, no. 1, pp. 8–20, Jan. 2001.

[7] F. Hu, J. Wu, L. Chang, and R. F. Hanssen, "Incorporating temporary coherent scatterers in multi-temporal InSAR using adaptive temporal subsets," *IEEE transactions on geoscience and remote sensing*, vol. 57, no. 10, pp. 7658–7670, 2019.

[8] B. M. Kampes, *Displacement parameter estimation using permanent scatterer interferometry*, Ph.D. thesis, Delft University of Technology, Delft, the Netherlands, 2005.